Surface passivation by embedment of polyphosphate inhibits the aragonite-to-calcite thermodynamic pump

Boyang Gao,† Kristin M. Poduska,* Shifi Kababya, Asher Schmidt*

Boyang Gao: Department of Chemistry, Memorial University of Newfoundland & Labrador, St. John's, NL, A1B 3X7, Canada

Kristin M. Poduska: Departments of Chemistry/ Physics & Physical Oceanography, Memorial University of Newfoundland & Labrador, St. John's, NL, A1B 3X7, Canada

Shifi Kababya: Schulich Faculty of Chemistry and The Russell Berrie Nanotechnology Institute, Technion – Israel Institute of Technology, Haifa 32000, Israel

Asher Schmidt: Schulich Faculty of Chemistry and The Russell Berrie Nanotechnology Institute, Technion – Israel Institute of Technology, Haifa 32000, Israel

KEYWORDS: calcium carbonate, dissolution, crystallization, solid-state NMR, REDOR, infrared spectroscopy

ABSTRACT: We monitor the conversion of aragonite to calcite in water by comparing single and mixed polymorph suspensions. We demonstrate that the enhanced aragonite-to-calcite conversion in mixed polymorph suspensions is dramatically inhibited by adding polyphosphate (sodium hexametaphosphate). ^{13}C and ^{31}P solid-state magic angle spinning (MAS) NMR and attenuated total reflectance Fourier transform infrared (ATR-FTIR) spectra allow us to follow quantitatively these effects as imparted by the dissolution-recrystallization processes. $^{13}C\{^{31}P\}$ rotational echo double resonance (REDOR) NMR experiments reveal coprecipitated phosphate that is embedded only within the surfaces of both polymorphs during the initial dissolution and recrystallization processes, causing passivation that arrests phase conversion.

The diagenesis of calcium carbonates, including their dissolution and recrystallization, is important in both marine and freshwater systems because of its impact on the ocean carbon budget,[1-3] ocean acidification[4-5] and for CO_2 capture and storage technologies.[6] Underlying these diagenetic factors, the two most common $CaCO_3$ polymorphs, (aragonite and calcite) have low – but different values for – equilibrium solubility constants.[7] In this work, we use solid-state NMR and infrared spectroscopy to follow the manifestation of calcite-to-aragonite phase conversion processes when powders of these two phases are co-suspended in water. Moreover, we identify at the molecular level a mechanism that inhibits the phase conversion: surface embedment of a dissolved phosphate-bearing additive. Thus, we probe the mechanistic interplay between fundamental processes of carbonate mineral dissolution and recrystallization, with relevance to biomineralization, geochemical and technological processes.

First, we highlight the pronounced impact that co-suspended calcite has on the dissolution of aragonite, and its subsequent crystallization as calcite. As reference samples, we use neat aragonite and neat calcite powders, which we compare with 1:1 mixtures of the two phases (synthesis details in SI). To track unequivocally the aragonite-to-calcite transformation by ^{13}C DE MAS (direct excitation magic angle spinning) NMR, we enriched the aragonite ^{13}C isotope content to 20%, while using calcite at natural abundance [n.a.] ^{13}C (1.1%). Thus, only calcite that forms from dissolved aragonite will have a significant ^{13}C NMR signature.

We start by examining the neat powders before and after suspension in water. The ^{13}C DE MAS NMR spectrum in Figure 1a shows a starting material that is comprised of 98% aragonite (peak at 170.7 ppm), with ~2% calcite byproduct (peak at 168.5 ppm).

After immersion in water for 1 week, the spectrum for this powder (Figure 1b) shows a minute change: 96% aragonite with 4% calcite suggests a small (2%) conversion of aragonite to calcite. ATR-FTIR experiments for even longer immersion times (3 weeks) do not show evidence of phase transformation (SI Figure S2). Similar control experiments with neat [20%-^{13}C] calcite (SI Figure S1) show no detectable back-conversion to aragonite. Hence, these data set a baseline for the temporal stability of neat aragonite and neat calcite suspensions in water.

A strikingly different situation is revealed after 1 week of immersion for the co-suspended aragonite and calcite powders. Figure 1c shows that ~55% of the starting aragonite dissolved and recrystallized as calcite. This trend is corroborated with ATR-FTIR spectra (Figure 2a-d and SI Figure S3c). The conversion from aragonite to calcite is rationalized by the slightly higher pK_{sp} of calcite *vs*. that of aragonite (8.48 vs. 8.34).[3,8] This difference forces the $CaCO_3$ activity

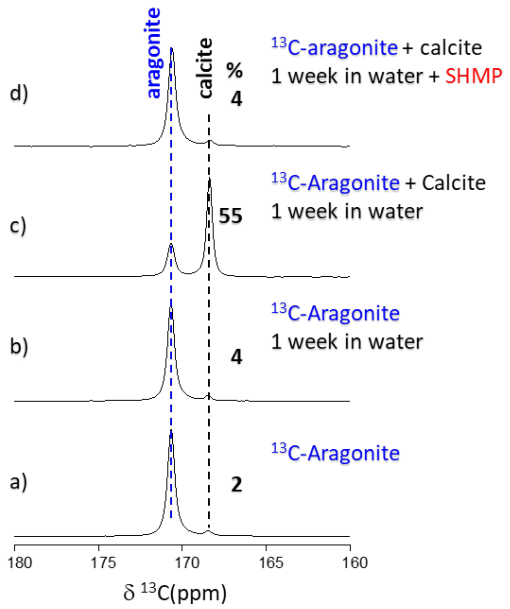

Figure 1. 75.4 MHz ^{13}C DE MAS spectra: (a) as-synthesized [20%-^{13}C] aragonite powder, and (b) after suspension in water; (c) 1:1 mixture of [20%-^{13}C] aragonite and [n.a.-^{13}C] calcite powders after suspension in either water or (d) 10 mM SHMP (sodium hexametaphosphate). ^{13}C calcite fractions greater than 2% indicate aragonite dissolution with subsequent crystallization as calcite. All spectra used 8-32 transients with 2400 s repetition delay to facilitate quantification.

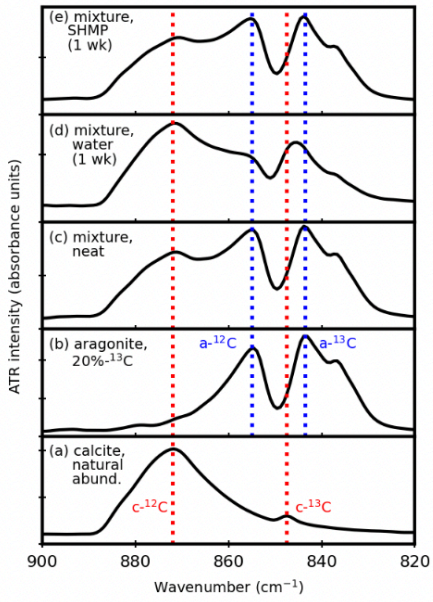

Figure 2. ATR-FTIR spectra of (a) [n.a.] calcite and (b) [^{13}C-20%] aragonite, and their 1:1 mixture (c). The spectra obtained after suspending this mixture in pure water (d) and in 10 mM SHMP (e), demonstrate the pronounced aragonite-to-calcite conversion in pure water, and its arrest in the SHMP solution. The spectra focus on the out-of-plane ν_2 carbonate vibrational mode, which is distinct for aragonite and calcite.[9]

product to lie in between the K_{sp} values for the two polymorphs: slightly supersaturated for calcite and slightly undersaturated for aragonite. Hence, aragonite dissolves to approach its K_{sp} value, while calcite crystallization consumes the dissolved ions to offset its supersaturation. This in turn elicits further aragonite dissolution.

ATR-FTIR data (SI Figure S3) show that higher fractions of calcite in the starting ratio yield larger aragonite fractions that converted to calcite after 1 week of suspension in water. This substantiates that calcite surfaces provide nucleation sites whose increased concentration enhances overgrowth, thereby promoting a more efficient thermodynamic aragonite-to-calcite pump.

Sodium hexametaphosphate (SHMP) is a common water softener agent and deflocculant. Remarkably, by dissolving this P-bearing additive (10 mM) in the aragonite-calcite mixture suspension, the aragonite-to-calcite phase conversion is fully arrested over the same 1 week time span. This is evident from the close similarity of the DE NMR spectra of the neat aragonite and the mixture + SHMP suspensions (Figure 1d and 1b), and the corresponding ATR-FTIR spectra (Figure 2e and 2c), indicative of the profound effect that SHMP has on the dissolution-recrystallization processes.

Seeking mechanistic insight for SHMP's role in suppressing the calcite-to-aragonite pump, we examine ^{31}P DE MAS NMR spectra for evidence of SHMP coprecipitation. Indeed, Figure 3a shows three characteristic ^{31}P peaks for SHMP that represent its hydrolysis products: Pi, pyrophosphate or terminal P species, and internal P species (centered at 4, -5, -20 ppm, respectively). The similar relative intensities among these three peaks in each spectrum confirm similar coprecipitated species abundances, whether from single-phase (calcite or aragonite) or 1:1 mixed-phase suspensions. Complementarily, inductively coupled plasma optical emission spectroscopy (ICP-OES) analyses show similar total levels of P-bearing species: 0.30 mol% with aragonite, 0.25 mol% with calcite, and 0.41 mol% with the 1:1 mixture (see also SI Table S1). The excessive breadth of the ^{31}P peaks in the DE NMR spectra indicates that these P-species are disordered, suggesting that they are dispersed, surface embedded or bound, rather than separated crystalline phases.[10] To substantiate this distinction, we opt for REDOR measurements.[11,12]

The $^{31}P\{^{13}C\}$ DE-REDOR experiment yields two spectra (Figure 3b). The first is a reference ^{31}P DE MAS spectrum, S_0, which accounts for all peaks; the second is a REDOR spectrum, S_R, with attenuated peaks for ^{31}P-species near carbonates (< 7Å $^{31}P\cdots^{13}C$ distance). Qualitatively, REDOR peak attenuation is more pronounced when the distance is shorter and/or when the fraction of such carbonate-proximate P-species is larger. As such, peak attenuation alone indicates the occurrence of phosphate⋯carbonate proximities that represent electrostatic interactions that are mediated by the positively charged Ca^{2+} ions.[13] Figure 3b shows the $^{31}P\{^{13}C\}$ DE-REDOR spectra of the of the three powders – neat aragonite, calcite, and mixture – after 1 week immersion in SHMP solution. Their reference spectra (S_0, black traces) show all three characteristic peaks of SHMP (as visible in the DE MAS spectra in Figure 3a). The S_R

spectra (Figure 3b; red traces) show notable attenuation of the Pi and pyro-/terminal peaks: 20±3% for the single polymorph powders, and 12±3% for the 1:1 mixture. Given that the neat aragonite and calcite are only 20%, ^{13}C-enriched, only 20% of the possible P-C proximity occurrences will be sensed by the ^{31}P-^{13}C REDOR measurement. Thus, the 20% attenuation in S_R indicates that all coprecipitated Pi and Pyro- and terminal phosphates are engaged in short-range interactions with the carbonates.

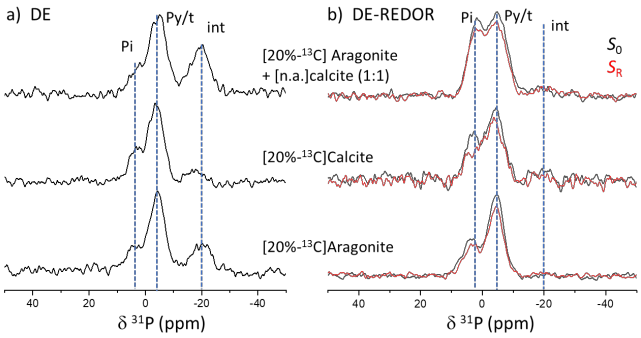

Figure 3. a) ^{31}P DE MAS NMR spectra of powders of [20%-^{13}C] aragonite, [20%-^{13}C] calcite and their 1:1 mixture of [20%-^{13}C] aragonite with calcite, after suspension in 10mM SHMP solution (1 week). Three hydrolysis products of SHMP appear: Pi, Pyro- and terminal phosphate, and internal phosphate are denoted Pi, Py/t, and int. b) 64T_R (6.4ms) ^{31}P{^{13}C} DE-REDOR spectra of the three powders; reference and REDOR spectra, S_0 and S_R, of each powder are overlayed in black and red, respectively. Spectra used a relaxation delay of 20s and spinning speed of 10 kHz.

For the 1:1 mixture wherein only the aragonite is ^{13}C-enriched, there is ~2 times less REDOR attenuation. Given the similar amounts of SHMP that coprecipitated with the neat polymorphs and the mixture. This observation is consistent with P-species being evenly distributed between the two polymorphs and exhibiting no polymorph preference. In this case only proximities involving the ^{13}C-enriched aragonite affect the REDOR attenuation, while proximities related to the calcite (^{13}C at 1.1%) have only negligible contribution, thereby reducing by 2-fold the overall attenuation for the mixture. Additional measurements show that by doubling the dipolar evolution time in the REDOR experiments (12.8 ms; 128T_R), the attenuation of the S_R spectra more than doubles (SI Figure S4). Exceeding the 20% ^{13}C enrichment level, which is the maximum attenuation that can be caused by a single carbonate neighbor, further establishes that all coprecipitated P-species interact with more than two carbonates in their immediate vicinity.

Taken together, the ^{31}P{^{13}C} DE-REDOR data rule out the occurrence of separate P-rich phases. Moreover, they unequivocally indicate that P-species are dispersed, *surface-embedded* or *surface-adsorbed*, consistent with their disordered nature as manifested by their broad peaks. To probe for carbonates that directly interact with P-species, ^{13}C{^{31}P} DE- and CP-REDOR measurements were attempted. That they yielded hardly detectable S_R attenuation (SI Figure S5) attests that only a small fraction of the carbonates is proximate to the P-bearing moieties. This result is perfectly in line with SHMP being embedded only within (or atop) the narrow surface layer that underwent dissolution-recrystallization, whereas the majority bulk carbonates do not interact with SHMP.

Our study clearly reveals the mechanism by which P-bearing additive molecules, which can be found readily in aqueous environments, are embedded within the dissolving-recrystallizing surfaces of calcite and aragonite, thereby passivate these surfaces, and inhibit the dissolution-recrystallization processes. We emphasize that additive-embedment alters the surface thermodynamics as well as the resulting dissolution-recrystallization kinetics. The decreasing phase conversion rates as function of time that we observe (Figure S6) are a manifestation that factors such as varying grain sizes and exposed facets are involved in the complex interplay between thermodynamics and kinetics.

Our data therefore suggest that surface embedment of SHMP during the initial dissolution-recrystallization of aragonite and calcite yields surfaces where the thermodynamic forces which drive the aragonite-to-calcite pump no longer prevail. This mode of action of P-species embedment is consistent with our earlier study[14] that identified that strong phosphate···carbonate interactions (Ca^{2+}-mediated) impeded $CaCO_3$ nucleation in solution, and their persistence in the amorphous calcium carbonate (ACC) solid also prevented its crystallization.[13]

Aragonite-to-calcite conversion in aqueous environments is a widespread phenomenon. One recent example considers this in benthic marine environments, exploring the kinetics as a function of different exposed crystalline faces.[3] However, possible implications of the time scales and inhibition strategies that could be relevant for mixed-polymorph environments are unexplored. For example, marine organisms use polyphosphates throughout biomineralization to regulate the properties and functions of calcium carbonate minerals.[15,16] Polyphosphate is also relevant for both carbonate mineralization and diagenesis in terrestrial geology,[17] and its role in preventing aragonite dissolution is of great importance when analyzing aragonite for radiocarbon dating.[18] In industrial settings, surface fouling by carbonate minerals is sometimes prevented by using polyphosphate antiscalants,[19] including those with eutrophic origins.[20]

Despite the vast interest in calcium carbonate phases and their surface stability in aqueous environments,[10,21-23] there is very little direct evidence on the mechanisms and the underlying molecular level principles that influence the tightly interdependent thermodynamic and kinetic processes that polyphosphate embedment has on the aragonite-to-calcite balance. To this end, our study provides a direct observation of the mechanism by which P-species are surface embedded, which then controls dissolution-recrystallization to halt aragonite-to-calcite phase conversion.

ASSOCIATED CONTENT

Supporting Information. Experiment details. Figure S1: DE NMR spectra of neat calcite after suspension in water. Figure S2: ATR-FTIR spectra of neat calcite and neat aragonite after longer periods of water suspension. Figure S3: ATR-FTIR spectra for different starting ratios of calcite: aragonite suspensions

in water. Figure S4: 128T_R $^{31}P\{^{13}C\}$ REDOR NMR spectra of neat calcite, neat aragonite, and their mixture after suspension in SHMP. Figure S5: $^{13}C\{^{31}P\}$ REDOR NMR spectra of neat calcite, neat aragonite, and their mixture after suspension in SHMP. Figure S6: NMR-based phase conversion rates. Table S1: ICP-OES data. This material is available free of charge via the Internet at http://pubs.acs.org.

AUTHOR INFORMATION

Corresponding Author

* Kristin Poduska (kris@mun.ca) and Asher Schmidt (asher@ch.technion.ac.il)

Present Addresses

† Section 9, No.188, the South Fourth Ring Road-West Road, Beijing 100070, China.

Author Contributions

The manuscript was written through contributions of all authors.

Funding Sources

K.M.P acknowledges NSERC (Canada) Discovery Grant 2018-04888. A.S. acknowledges the Israel Science Foundation grant 2001/17 for financial support.

ABBREVIATIONS

ATR-FTIR: attenuated total reflection Fourier transform infrared; DE MAS NMR: direct excitation magic angle spinning nuclear magnetic resonance; ICP-OES: inductively coupled plasma optical emission spectroscopy; [n.a.]: natural abundance; REDOR: rotational echo double resonance; SHMP: sodium hexametaphosphate.

REFERENCES

1. Palmer, T.J.; Wilson, M.A. Calcite precipitation and dissolution of biogenic aragonite in shallow Ordovician calcite seas. *Lethaia.* **2004** *37*, 417-427. DOI: 10.1080/00241160410002135
2. Dong, S.; Berelson, W. M.; Rollins, N. E.; Subhas, A. V.; Naviaux, J. D.; Celestian, A. J.; Liu, X.; Turaga, N.; Kemnitz, N. J.; Byrne, R. H.; Adkins, J. F. Aragonite dissolution kinetics and calcite/aragonite ratios in sinking and suspended particles in the North Pacific. *Earth Planet. Sci. Lett.* **2019**, *515*, 1-12. DOI: 10.1016/epsl.2019.03.016
3. Sulpis, O.; Agrawal, P.; Wolthers, M.; Munhoven, G.; Walker, M.; Middelburg, J. J. Aragonite dissolution protects calcite at the seafloor. *Nature Comm.* **2022**, *13*, 1104. DOI: 10.1038/s41467-022-28711-z
4. Bednaršek, N.; Tarling, G. A.; Bakker, D. C. E.; Fielding, S.; Feely, R. A. Dissolution Dominating Calcification Process in Polar Pteropods Close to the Point of Aragonite Undersaturation. *PLoS ONE* **2014**, *9 (10),* e109183. DOI: 10.1371/journal.pone.0109183
5. Janisezawka, K.; Mazur, M.; Machalski, M.; Stolarski, J. rom pristine aragonite to blocky calcite: Exceptional preservation and diagenesis of cephalopod nacre in porous Cretaceous limestones. *PLoS ONE,* **2018**, *13 (12),* e0208598. DOI: 10.1371/journal.pone.0208598
6. Kaufmann, G.; Dreybrodt, W. Calcite dissolution kinetics in the system $CaCO_3$–H_2O–CO_2 at high undersaturation. *Geochim. Cosmochim. Acta* **2007**, *71*, 1398-1410. DOI: 10.1016/j.gca.2006.10.024
7. Simmer, R. A.; Jansen, E. J.; Patterson, K. J.; Schnoor, J. L. Climate Change and the Sea: A Major Disruption in Steady State and the Master Variables, *ACS Envi*ron. Au **2023**, in press, accepted manuscript. DOI: 10.1021/acsenvironau.2c00061 (accessed 2023-07-17).
8. Boon, M.; Rickard, W. D. A.; Rohl, A. L.; Jones, F. Stabilization of Aragonite: Role of Mg^{2+} and Other Impurity Ions. *Cryst. Growth Des.* **2020**, *20*, 5006–5017. DOI: 10.1021/acs.cgd.0c00152
9. Weiner, S. Microarchaeology: Beyond the Visible Archaeology Record;, Cambridge University Press, **2012,** 284.
10. Sø, H. U.; Postma, D.; Jakobsen, R.; Larsen, F. Sorption of phosphate onto calcite; results from batch experiments and surface complexation modeling. *Geochim. Cosmochim. Acta.* **2011**, *75,* 2911–2923. DOI: 10.1016/j.gca.2011.02.031
11. Gullion, T.; Schaefer, J. Rotational-Echo Double-Resonance NMR. *J. Magn. Reson*. **1989**, *81 (1),* 196–200. DOI: 10.106/0022-2364(89)90280-1
12. Gullion, T.; Schaefer, J. Detection of Weak Heteronuclear Dipolar Coupling by Rotational-Echo Double-Resonance Nuclear Magnetic Resonance. *Adv. Magn. Opt. Reson*. **1989**, *13,* 57–83. DOI: 10.1016/B978-0-12-025509.50009-4
13. Kababya, S.; Gal, A.; Kahil, K.; Weiner, S.; Addadi, L.; Schmidt, A. Phosphate–Water Interplay Tunes Amorphous Calcium Carbonate Metastability: Spontaneous Phase Separation and Crystallization vs Stabilization Viewed by Solid State NMR. *J. Am. Chem. Soc.* **2015,** *137*, 990-998. DOI: 10.1021/ja511869g
14. Duchstein, P.; Schodder, P. I.; Leupold, S.; Dao, T. Q. N.; Kababya, S.; Cicconi, M.; de Ligny, D.; Pipich, V.; Eike, D.; Schmidt, A.; Zahn, D.; Wolf, S. E. Small-Molecular-Weight Additives Modulate Calcification by Interacting with Prenucleation Clusters on the Molecular Level. *Angew. Chem. Int. Ed.* **2022**, *61*, e202208475. DOI: 10.1002/anie.202208475
15. Gal, A.; Sorrentino, A.; Kahil, K.; Pereiro, E.; Faivre, D.; Scheffel, A. Native-state imaging of calcifying and noncalcifying microalgae reveals similarities in their calcium storage organelles. *Proc. Natl. Acad. Sci*. **2018**, *115 (43)* 11000. DOI: 10.1073/pnas.1804139115
16. Akiva-Tal, A.; Kababya, S.; Balazs, Y. S.; Glazer, L.; Berman, A.; Sagi, A.; Schmidt, A. In situ molecular NMR picture of bioavailable calcium stabilized as amorphous $CaCO_3$ biomineral in crayfish gastroliths. *Proc. Natl. Acad. Sci.* **2011**, *108 (36),* 14763-14768. DOI: 10.1073/pnas.1102608108
17. Wan, B.; Huang, R.; Diaz, J. M.; Tang, Y. Rethinking the biotic and abiotic remineralization of complex phosphate molecules in soils and sediments. *Sci. Total Environ.* **2022**, *833*, 155187. DOI: 10.1016/j.scitotenv.2022.155187
18. Toffolo, M. B. The significance of aragonite in the interpretation of the microscopic archaeological record. *Geoarchaeol.* **2020**, 1-21. DOI: 10.1002/gea.21816
19. Jafar Mazumder, M. A. A Review of Green Scale Inhibitors: Process, Typles, Mechanism and Properties. *Coatings* **2020**, *10*, 928. DOI: 10.3390/coatings10100928
20. Regulation (EC) No 648/2004 of the European Parliament and of the Council on Detergents, http://faolex.fao.org/docs/pdf/eur42319.pdf, last accessed 04 October 2023.
21. Bano, A. M.; Rodger, P. M.; Quigley. D. New Insight into the Stability of $CaCO_3$ Surfaces and Nanoparticles via

Molecular Simulation. *Langmuir* **2014**, *30*, 7513-7521. DOI: 10.1021/la501409j
22. Hadjittofis, E.; Vargas, S. M.; Litster, J. D.; Sedransk Campbell, K. L. The role of surface energy in the apparent solubility of two different calcite crystal habits. *Proc. R. Soc. A* **2021**, *477*, 20210200. DOI: 10.1098/rspa.2021.0200
23. Armstrong, B.; Silvestri, A.; Demichelis, R.; Raiteri, P.; Gale, J. Solubility-consistent force field simulations for aqueous metal carbonate systems using graphical processing units. *Phil. Trans. R. Soc. A* **2023**, *381*, 2022050. DOI: 10.1098/rsta.2022.0250

Surface dissolution-recrystallization processes drive aragonite-to-calcite phase conversion. Polyphosphate, when present, is embedded in the aragonite and calcite surfaces, halting these processes and arresting phase conversion.